Constraining structural dip and magnetization direction of a sheet from its static and dynamic magnetic anomalies

Clive Foss
CSIRO Mineral Resources
North Ryde, Sydney
Clive.foss@csiro.au

David Clark
CSIRO Manufacturing
Lindfield, Sydney
David.clark@csiro.au

Shane Keenan
CSIRO Manufacturing
Lindfield, Sydney
Shane.keenan@csiro.au

Keith Leslie
CSIRO Manufacturing
Lindfield, Sydney
Keith.Leslie@csiro.au

SUMMARY

Following advances in magnetometer instrumentation and inversion software we re-explore the feasibility of a field methodology utilising relationships between magnetization and dynamic (time-variation) magnetic field anomalies to recover structural information from magnetic field data over thin sheets. We show that we can estimate the dip of a sheet from a reliably determined dynamic magnetic anomaly induced by the range of the magnetic field through its diurnal variation. The strength and inclination of remanent magnetization in the plane perpendicular to the sheet can be subsequently estimated from the static magnetic anomaly using that pre-determined dip angle. The principal challenge in working with dynamic magnetic anomalies is their low amplitude and the requirement for multiple measurements at each station. These relationships between magnetizations and fields apply equally to field gradients. SQUID magnetometers and gradiometers can provide a feasible solution to the high resolution measurements required for this application

Key words: SQUID magnetic anomaly sheet remanent magnetization time-variation.

INTRODUCTION

For thin sheets of large depth and strike extent ('2-D' bodies) there are severe restrictions in recovering magnetization direction from magnetic field data. Components of magnetization parallel to the strike of the sheet do not contribute to the magnetic field anomaly and are therefore undetectable. Furthermore, the angle of structural dip and the apparent inclination of magnetization in the plane perpendicular to the sheet combine into a single term from which they cannot be individually recovered (Hall, 1959; Emerson at el., 1985; McGrath and Hood, 1970; Clark, 2014). Various methods have been previously proposed to try to overcome this problem through measurement of time-variation (dynamic) anomalies which are known or assumed to be due to induced magnetization only (Goldstein and Ward, 1966; Parkinson and Barnes, 1985; Clark et al., 1998; Clark, 2014). Inversion of a dynamic anomaly can recover an estimate of the dip of a sheet, and the direction of magnetization in the plane perpendicular to the sheet can then be derived from the static anomaly. Although exploitation of these relationships has been an objective for some time, this has not yet been achieved because of limited sensitivity of field magnetometers and gradiometers. However, new developments in SQUID instrumentation may now provide the required sensitivity.

THE HELLS DOORWAY SYNCLINE ANOMALY, EGERTON WA

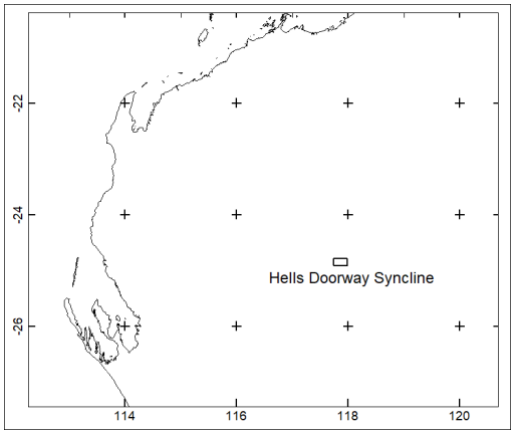

Figure 1. Location of the Hells Doorway Syncline, WA.

Figure 1 shows the location of the Hells Doorway Syncline near Egerton in West Australia. Total magnetic intensity (TMI) and geology maps of the syncline are shown in Figures 2 and 3 (at the end of the paper). The syncline is covered by a magnetic survey with north-south flight-lines at 500 metres spacing and a nominal 60 metres terrain clearance. The magnetic source of the anomaly can be represented as a thin sheet extending continuously between the northern and southern limbs of the fold. This magnetization distribution lies within the Middle Proterozoic Ullawarra Formation, reported to consist of arenite, siltstone, shale and dolomite (Muhling et al., 1978).

Figure 4 shows a modelled north-south flight-line across the centre of the anomaly. The northern flank anomaly has a peak to trough amplitude of 580 nT and the southern flank anomaly has an amplitude of 230 nT. Surface dips measured close to the profile report values on the northern limb of 72° and 80° to the south, and on the southern limb 40° and 70° to the north. The anomaly has been modelled using two tabular bodies with horizontal tops. The bodies were given appropriate strike extent and azimuth to match the trend of the anomaly in plan view, and a 2nd order polynomial of low curvature was adjusted to represent the background field as assumed would be measured if the anomalous magnetization were not present. The best-estimate magnetic susceptibility, depth, thickness, distance

along profile, depth extent and dip of the tabular bodies were then found by multi-parameter inversion.

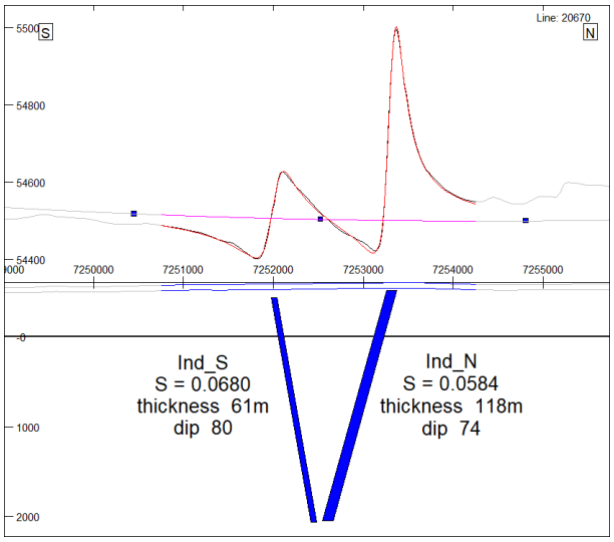

Figure 4. Best-fit induced magnetization model for line 20670 (location shown in Figures 2 and 3).

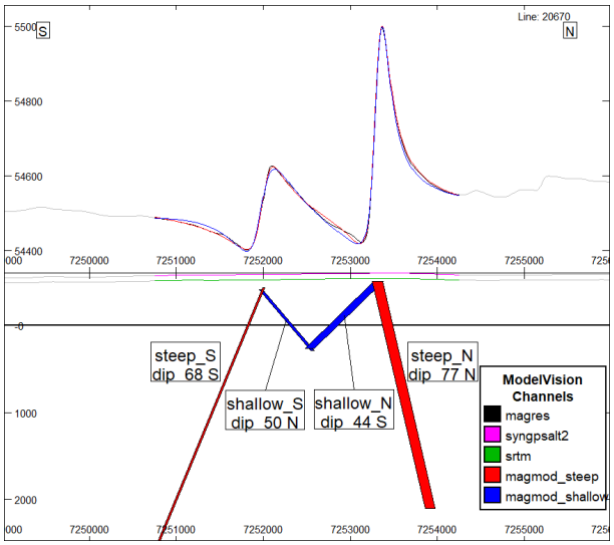

Figure 5. Alternative models with sheet dips 30° shallower (blue) and steeper (red).

A magnetic sheet anomaly can be matched with a resultant (induced plus remanent) magnetization across a wide range of magnetization directions with each direction linked to a particular dip of the sheet. Neglecting interference from neighbouring anomalies, the angle between the down-dip direction and the magnetisation direction in the plane normal to strike is identical for all such equivalent sheets. Figure 5 shows model sections for bodies with dips rotated by 30° to those of the induced magnetization bodies. Inversion was used to find the corresponding resultant magnetizations of the sheets, with directions constrained to the plane perpendicular to strike. The remanent contribution to the magnetization is not uniquely determined from the resultant magnetizations, which can either be predominantly remanent with a direction close to the resultant, or have a smaller remanent component with a more separated direction. In this study we set remanent and induced magnetizations to be of similar strength ($Q \approx 1$). Magnetization directions of the models are shown in Figure 6. Because the directions are perpendicular to the near east-west trend of the sheets they fall in a north-south swathe, and because $Q \approx 1$ the remanent directions are twice as far removed from the magnetic field direction as are the resultant directions. There is little discrimination between the models from their near-identical static magnetic field anomalies, but dynamic magnetic anomaly data can provide this discrimination.

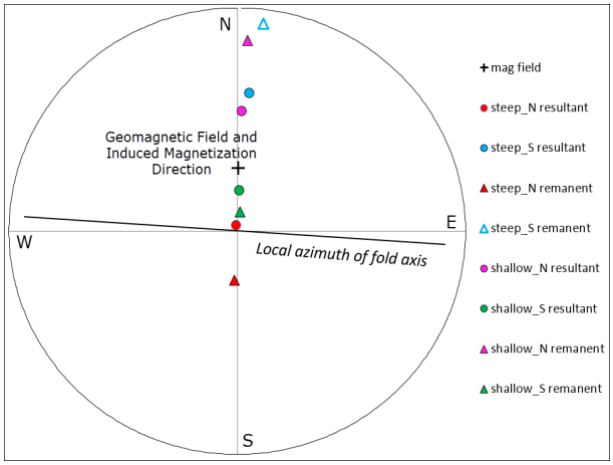

Figure 6. Magnetization directions of the north and south fold limbs for the steeper and shallower dip models.

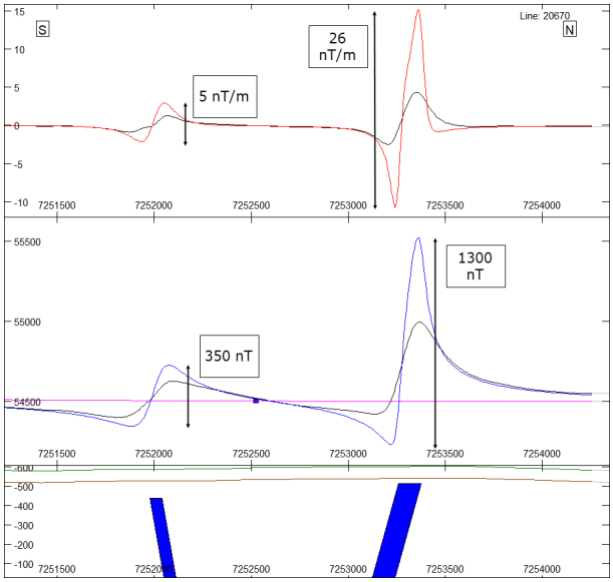

Figure 7. Magnetization directions of the north and south fold limbs for the steeper and shallower dip models.

Figure 7 shows the magnetic anomaly of the induced model computed at ground elevation to simulate a ground magnetic traverse. The northern and southern anomalies have peak to trough amplitudes of 1300 nT and 350 nT respectively, with corresponding amplitudes of 26 nT/m and 5 nT/m for the vertical gradient of TMI anomalies.

All of the above models were computed for a geomagnetic field strength of 54615 nT. We also forward computed the fields from the models for a slightly stronger geomagnetic field of 54670 nT (an increase of 55 nT) with the same direction. This does not result in a consistent displacement of the anomalies by 55 nT because there is amplification of the induced magnetization contribution to the anomalies resulting from the increase in strength of the inducing field.

Figure 8 plots the dynamic anomalies as defined by the difference between anomalies in the two inducing fields. For the induced-only model the shape of the dynamic and static anomalies are identical because both the magnetization directions and geometries are identical. The shape of all 3 dynamic anomalies are different because while the models have identical magnetization directions, their geometries are different. The amplitude of the induced-only model is higher than for the other models because all of the magnetization of the induced-only model contributes to the dynamic anomaly, while only part of the magnetization of the other models contributes. The amplitudes of the dynamic anomalies are important because they indicate what precision of measurement is required for their analysis. For the northern limb anomaly with ranges of over 1 nT and over 10 pT/m for the dynamic field and gradient anomalies respectively, measurement precisions of 100 pT and 1 pT/m would be required, but for the southern limb anomaly required precisions are clearly higher. The relative merits of working with fields or gradients depends on specifics of the instrumentation and depth to the top of magnetization (with gradiometry having relative advantage for shallower magnetizations). Unfortunately Australia has generally low quiet-day diurnal variations (of advantage for static field studies, but a draw-back to dynamic anomalies) and a range of 50 nT will not be observed on many days.

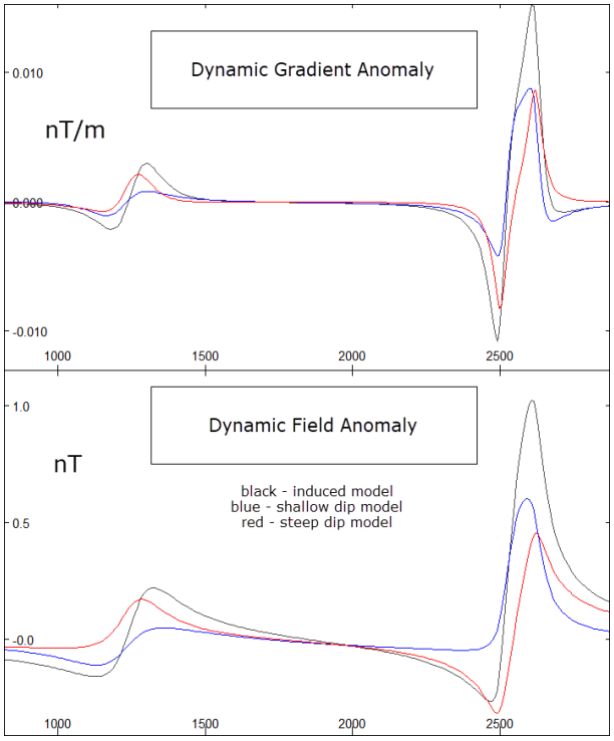

Figure 8. Dynamic anomalies of the field and vertical gradient.

The dynamic anomalies are due only to induced magnetization and can be inverted using that known magnetization direction. In each case the model dips are recovered from the inversions. Furthermore, the contribution to the static anomalies from induced magnetization can be estimated by scaling the dynamic anomalies by the ratio of the strength of the static field to the range between the two fields. The numerical stability of this estimate is dependent on the quality with which the dynamic anomaly is defined (because the scaling factor is so high - in this case 1000:1). The contribution of remanent magnetization to the static anomaly is derived by subtracting the induced magnetization contribution from the estimated resultant magnetization.

RESOLUTION CAPABILITIES OF CSIRO SQUID MAGNETOMETERS AND GRADIOMETERS

In general, geomagnetic time variations affect all three components of the field. Maximum information about the sources is obtained using a vector base station that monitors changes in X, Y and Z components of the field. Modern atomic magnetometers are very sensitive (sub-pT resolution) and are insensitive to small changes in orientation that may occur over hours or days, but only effectively measure a single component of the diurnal variation (that parallel to the regional field). Vector magnetometers, such as fluxgates and SQUIDs are very sensitive to motion noise on moving platforms, but can accurately measure triaxial geomagnetic variations in base station mode, particularly if sensitive tiltmeters are incorporated into the sensor package, to correct for vibrations and for slow tilting. Drift of sensor base levels ($1/f$ noise) can adversely affect the proposed method, but these can be effectively eliminated by using rotating sensor designs as developed by CSIRO (Tilbrook, 2004; Leslie et al., 2007; Keenan et al., 2015). Given the relatively long integration times available for this application, sensitivities better than 1 pT should be attainable for field component measurements using high-T SQUIDs. Platform stability and tilt measurement are the limiting factors on attainable accuracy, rather than sensor noise. With a high-T SQUID gradiometer system and integration times of 10-100 seconds, sensitivities of ~ 1 pT/m should be attainable, which should be sufficient to detect time-varying gradients for many anomalies. The full tensor magnetic gradiometer developed at CSIRO [Keenan et al., 2013; Billings et al., 2012] using a static arrangement of six high-Tc planar SQUID gradiometers on a hexagonal pyramid ,as shown in Figure 9, has a gradient field sensitivity of better than 2 pT/m/√Hz in unshielded stationary measurements. This system also incorporates a set of 3 axis SQUID magnetometers, with typical sensitivities of ~200 fT/√Hz, for background field referencing which additionally can be used to correlate to base station measurements.

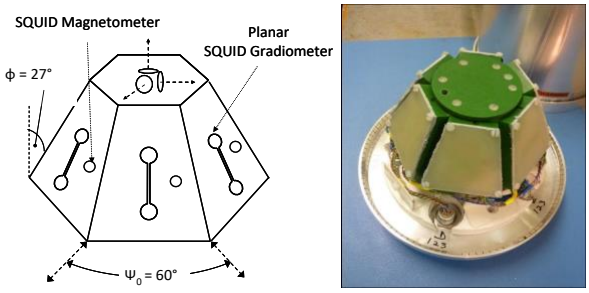

Figure 9. Schematic (left) and photo (right) of the full tensor magnetic gradiometer which uses six planar SQUID gradiometers with multiple reference sensors.

PLANNED FIELD PROCEDURE

We envisage that a field study of a selected aeromagnetic anomaly will first involve measurement of a ground traverse to select 5 to 10 suitable sites (10 to 20 sites for the double anomaly profile in this study) plus an off-anomaly base-station. Each site will have a plinth for exact re-location of the SQUID magnetometer/gradiometer. A caesium vapour magnetometer

and a triaxial fluxgate with tiltmeter should be sufficient for the base-station. Over a period of one or more days, and towards times of maxima and minima in the diurnal variation, each site will be re-visited multiple times. On each occasion a measurement sequence of 5 to 10 minutes should be sufficient to select a consistent subset of data at both the base-station and field-station with which to tag a field-station value against a corresponding base-station value of the total field and/or individual field components. Variation at each field-station will be normalised to a consistent base-station range of the field or components (most probably between the minimum of maxima base-station values and the maximum of minima base-station values tagged for each station). This set of normalised ranges at each field-station defines the dynamic anomaly. Data analysis requires inversion of the dynamic anomaly (using an assumption of induced magnetization and a background field of amplitude equal to the base-station range) to resolve source geometry. That geometry and magnetic susceptibility value will be used in an inversion of the static magnetic anomaly to resolve components perpendicular to the strike of the sheet of both resultant and remanent magnetization.

CONCLUSIONS

We have demonstrated the basis of one method of dynamic magnetic anomaly analysis and how this can be used to determine the structural dip of a thin sheet and the component of remanent magnetization in the plane perpendicular to the sheet. Application of field studies will depend on the resolution and repeatability with which measurements can be made to meet the demands of low amplitude signals (of the order of $1/1000^{th}$ of the amplitude of corresponding static anomalies). SQUID magnetometers and gradiometers developed at CSIRO have sufficient sensitivity to detect time-varying gradients for most anomalies of interest.

REFERENCES

Billings et al, 2012. Superconducting Magnetic Tensor Gradiometer System for Detection of Underwater Military Munitions, SERDP Project MR-1661.

Clark, D. A., Schmidt, P. W., Coward, D. A. and Huddleston, M. P., 1998. Remote determination of magnetic properties and improved drill targeting of magnetic anomaly sources by Differential Vector Magnetometry (DVM). Exploration Geophysics, 29, 312-319.

Clark, D.A., 2014. Methods for determining remanent and total magnetisations of magnetic sources - a review. Exploration Geophysics, 45, 271–304. http://dx.doi.org/10.1071/EG14013.

Emerson, D. W., Clark, D. A., and Saul, S. J., 1985, Magnetic exploration models incorporating remanence, demagnetisation and anisotropy: HP 41C handheld computer algorithms: Exploration Geophysics, 16, 1–122. doi:10.1071/EG985001

Goldstein, N.E. and Ward, S.H., 1966. The separation of remanent from induced magnetization in situ. Geophysics, 31, 779-796.

Hall, D.H., 1959, Direction of polarization determined from magnetic anomalies: Journal of Geophysical Research, 64, 1945-1959. doi:10.1029/JZ064i011p01945

Keenan, S.T., Du, J., Mitchell, E.E.,, Lam, K.H., Macfarlane, J.C., Lewis, C.J., Leslie, K.E., and Foley, C.P., 2013. High-Tc Superconducting Electronic Devices Based on YBCO Step-Edge Grain Boundary Junctions IEICE Trans. Electron., VOL.E96–C, NO.3.

Keenan, S., Leslie, K., and Clark, D., 2015. Single sensor HTS SQUID magnetic tensor gradiometer. In: European Conference on Applied Superconductivity (EUCAS); 6-10 September; Lyon, France. IEEE Transactions on Applied Superconductivity; 2015. 1. https://publications.csiro.au/rpr/download?pid=csiro:EP152283&dsid=DS5

Leslie, K., Blay, K.; Clark, D., Schmidt, P., Tilbrook, D., and Foley, C. P., 2007. Helicopter trial of magnetic tensor gradiometer. 19th International Geophysical Conference & Exhibition (ASEG 2007); Perth, WA.

McGrath, P. H., & Hood, P. J. (1970). The dipping dike case: a computer curve-matching method of magnetic interpretation. Geophysics, 35(5), 831-848.

Muhling, P.C., Brakel, A.T., and Davidson, A.W., 1978, Mount Egerton, Western Australia Sheet SG50-3, 1:250,000 explanatory series, Geological Survey of Western Australia.

Parkinson, W.D. and Barnes, C.D., 1985. In situ determination of Koenigsberger ratio. Australian Journal of Earth Science, 32, 1-5.

Tilbrook, D.L., 2004. The design of a new concept HTSC axial gradiometer. Physica C, 407, 1-9.

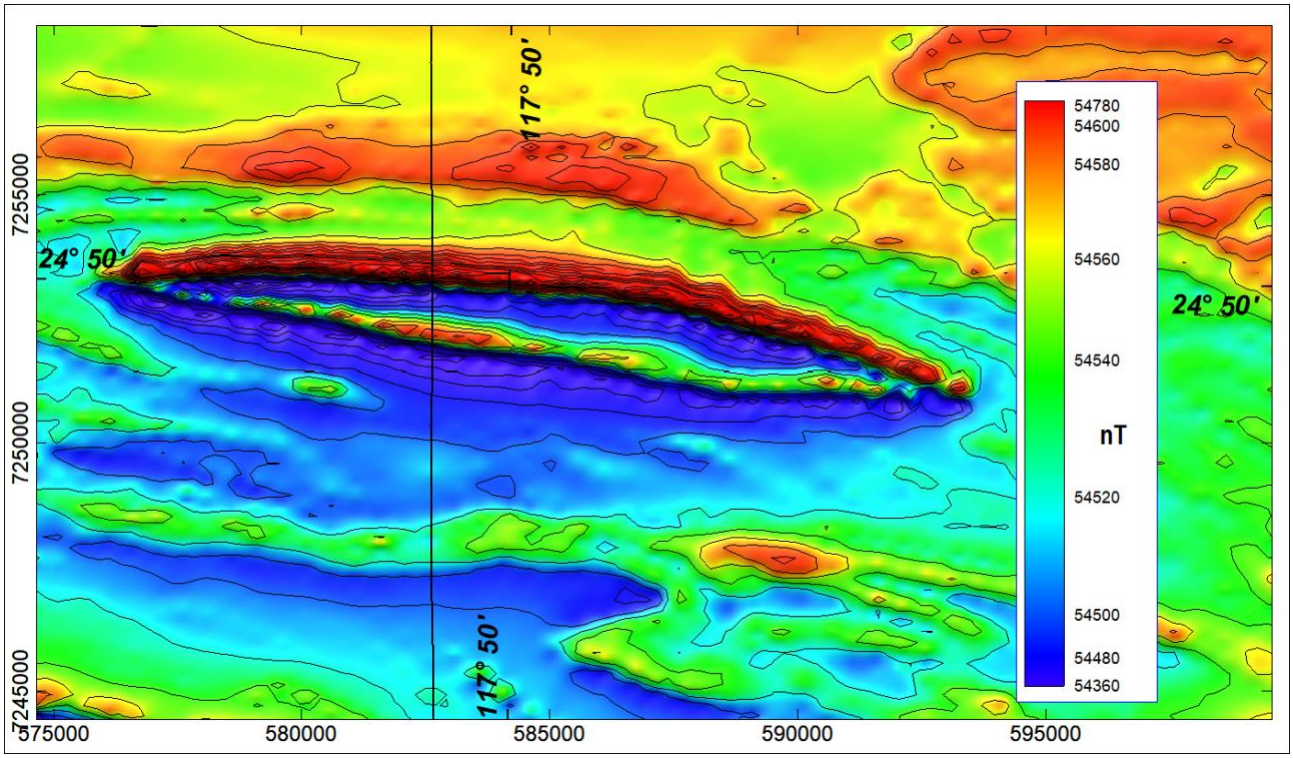

Figure 2. TMI anomaly with location of line 20670.

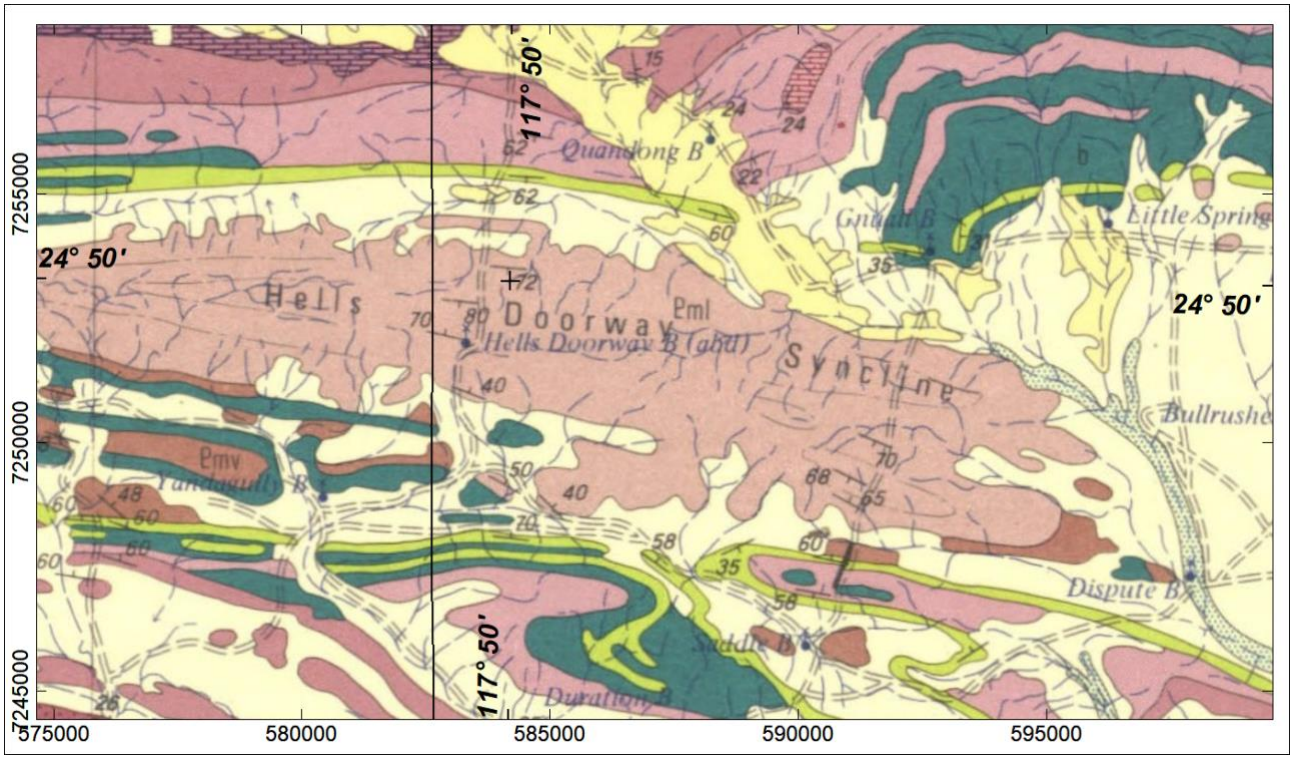

Figure 3. Geological map (Muhling et al., 1978) with location of line 20670 [Pml = Ullawarra Formation].